Natural Resources Canada
Ressources naturelles Canada

Surficial geology and Holocene shoreline evolution near Whitebeach Point, Great Slave Lake, Northwest Territories

H.B. O'Neill, S.A. Wolfe, and D.E. Kerr

Geological Survey of Canada
Current Research 2019-3

2019

Canada

Geological Survey of Canada
Current Research 2019-3

Surficial geology and Holocene shoreline evolution near Whitebeach Point, Great Slave Lake, Northwest Territories

H.B. O'Neill, S.A. Wolfe, and D.E. Kerr

2019

ISSN 1701-4387
ISBN 978-0-660-30510-3
Catalogue No. M44-2019/3E-PDF
https://doi.org/10.4095/314638

A copy of this publication is also available for reference in depository libraries across Canada through access to the Depository Services Program's Web site at http://dsp-psd.pwgsc.gc.ca.

This publication is available for free download through GEOSCAN (https://geoscan.nrcan.gc.ca).

Recommended citation

O'Neill, H.B., Wolfe, S.A., and Kerr, D.E., 2019. Surficial geology and Holocene shoreline evolution near Whitebeach Point, Great Slave Lake, Northwest Territories; Geological Survey of Canada, Current Research 2019-3, 15 p. https://doi.org/10.4095/314638

Critical review

P. Morse

Authors

H.B. O'Neill (hughbrendan.oneill@canada.ca)
S.A. Wolfe (stephen.wolfe@canada.ca)
D.E. Kerr (daniel.kerr@canada.ca)
Geological Survey of Canada
601 Booth Street
Ottawa, Ontario
K1A 0E8

Correction date:

Surficial geology and Holocene shoreline evolution near Whitebeach Point, Great Slave Lake, Northwest Territories

O'Neill, H.B., Wolfe, S.A., and Kerr, D.E., 2019. Surficial geology and Holocene shoreline evolution near Whitebeach Point, Great Slave Lake, Northwest Territories; Geological Survey of Canada, Current Research 2019-3, 15 p. https://doi.org/10.4095/314638

Abstract: Deposits of well sorted silica-rich beach sands occur along the western shore of Great Slave Lake around Whitebeach Point, Northwest Territories. Much of these deposits were windblown and redeposited following Holocene regression of glacial Lake McConnell and ancestral Great Slave Lake. Eolian deposits include active and stabilized sand sheets, transverse dunes, and localized blow-outs. High-resolution lidar and optical imagery, combined with optical and radiocarbon dating, were used to derive a lake-level regression curve for the area, map the surficial geology and geomorphology, and reconstruct Holocene shorelines and landscape development. Lake water level was near the base of a lime-stone escarpment in the study area ca. 9.5 ka, about 60 m above the present lake level, and subsequently declined at a rate of about 2.3 mm a^{-1} from ca. 7.0 ka onward. Lake-level regression was accompanied by beach- and eolian-sand deposition in the form of incipient foredunes, primarily within a protected embay-ment. Permafrost occurs beneath land surfaces with thick (>30 cm) organic cover, including peatlands and densely forested areas, and likely affects the groundwater hydrology in the area. Permafrost is absent under sparsely vegetated eolian sand surfaces.

Résumé : On trouve des dépôts bien triés de sable de plage riche en silice le long de la rive ouest du Grand lac des Esclaves, à proximité de la pointe Whitebeach (Territoires du Nord-Ouest). La majeure partie de ces dépôts ont été emportés par le vent et resédimentés après la régression du Lac glaciaire McConnell et du proto-Grand lac des Esclaves au cours de l'Holocène. Les dépôts éoliens comprennent des nappes de sable actives et stabilisées, des dunes transversales et des creux de déflation localisés. Nous avons utilisé de l'imagerie lidar haute résolution et de l'imagerie optique en combinaison avec des datations optiques et au radiocarbone pour dériver une courbe de régression du niveau du lac dans la région, cartographier la géologie des formations superficielles et la géomorphologie et reconstituer les rives lacustres et l'évolution du paysage au cours de l'Holocène. Dans la région d'étude, le niveau du lac se situait près de la base d'un escarpement de calcaire à environ 9,5 ka, soit à quelque 60 m au-dessus de son niveau actuel, et s'est subséquemment abaissé à une vitesse d'environ 2,3 mm/a à partir de 7 ka envi-ron. La baisse du niveau du lac a été accompagnée par le dépôt de sable de plage et de sable éolien, sous la forme d'avant-dunes embryonnaires, principalement dans une échancrure protégée de la rive du lac. Du pergélisol est présent sous les surfaces émergées possédant une épaisse couverture organique (>30 cm), dont des tourbières et des aires densément boisées, et influe probablement sur l'hydrologie souterraine de la région. Le pergélisol est absent sous les surfaces de sable éolien à végétation clairsemée.

INTRODUCTION

Large proglacial lakes previously occupied vast regions in Canada (Prest et al., 1968), helping shape modern landscapes and landforms. Glacial Lake McConnell once covered 15% of the Northwest Territories (Wolfe et al., 2017), but prior to the last decade, relatively little was known about the surficial geology, Holocene paleogeography, or permafrost conditions associated with the lake's regression. Earlier surficial geological mapping focused on areas of southern Great Slave Lake (e.g. Lemmen, 1990), eastern Great Slave Lake (e.g. Kerr et al., 2014), and the Mackenzie River valley region to the west (Rutter et al., 1980, and adjoining maps). Paleogeographic studies on glacial-ice extent and glacial-lake history were largely restricted to national-scale summaries (Dyke et al., 2003; Prest et al., 1968), regional overviews (e.g. Craig, 1965; Lemmen et al., 1994; Smith, 1994), and targeted studies in the Slave River and Hay River areas (Vanderburgh and Smith, 1988). Similarly, information on permafrost conditions was primarily from early studies by R.J.E. Brown (e.g. Brown, 1973, 1966) and unpublished engineering reports (*see* references in Wolfe, 1998).

A renewed interest in this region stems in part from risks to northern development from the impacts of climate change, and the necessity of improved surficial-geology information for infrastructure planning, mineral exploration, and development. Recent surficial-geology mapping has employed remote predictive methods (Ednie et al., 2014; Morse et al., 2016a; Stevens et al., 2017), airphoto interpretation (Kerr et al., 2016, 2017; Kerr and O'Neill, 2017, 2018a, 2018b), and field-based surveys (Oviatt and Paulen, 2013; Paulen et al., 2017), and is ongoing in previously unmapped areas. In addition, permafrost ground-thermal and ground-ice conditions have recently been examined in detail in the Great Slave region (Karunaratne et al., 2008; Morse et al., 2016b; Wolfe et al., 2018; Wolfe and Morse, 2017).

The purpose of this research was to develop an understanding of the surficial geology and landscape development in lower-elevation areas surrounding Great Slave Lake. The western shoreline of Great Slave Lake provides an opportunity to contribute to the understanding of Holocene shoreline evolution because a series of beach ridges and eolian deposits have been preserved and can be dated using optical techniques. The study area is immediately south of Whitebeach Point, Northwest Territories. The specific objectives of this report are to (1) map the surficial geology and geomorphic features in the area, (2) reconstruct Holocene shoreline positions as the lake level regressed, and (3) infer the landscape development based on field evidence and other available information.

BACKGROUND

Glacial Lake McConnell

During the retreat of the Laurentide Ice Sheet in Canada, large proglacial lakes were impounded along the northwestern ice margin beginning about 13.0 ^{14}C ka BP (ca. 15.8 ka cal. BP) (Duk-Rodkin and Lemmen, 2000; Lemmen et al., 1994). Glacial Lake McConnell was the second largest of these water bodies, occupying the combined basins of Great Bear, Great Slave, and Athabasca lakes during its maximum stage about 10.5 to 10.0 ^{14}C ka BP (ca. 13 ka cal. BP; Lemmen et al., 1994; Smith, 1994). The lake boundaries evolved during deglaciation in response to the receding ice margins, glacio-isostatic rebound, and topographic configuration. Lake-level regression and terrestrial emergence occurred around the Great Slave Lake basin, with greater rates of rebound moving eastward (Lemmen et al., 1994). Lake levels receded rapidly prior to 9.0 ka cal. BP, and thereafter more slowly at rates between 2 and 5 mm a^{-1} (Smith, 1994; Wolfe and Morse, 2017). Glacial Lake McConnell affected the regional geomorphology by reworking submerged till and depositing widespread fine-grained lacustrine sediments (Stevens et al., 2017; Wolfe et al., 2017). Holocene permafrost development in lacustrine sediments in the Great Slave Lowlands around Yellowknife has resulted in the widespread formation of raised ice-cored ridges and mounds known as lithalsas, and the thaw of these features has affected infrastructure stability in the region (Wolfe et al., 2014).

Study area

The study area is on the western shoreline of Great Slave Lake, extending south from Whitebeach Point (lat. 62.468°N; long. 115.253°W) for about 6 km (Fig. 1). It is situated within the Taiga Plains High Boreal Ecoregion and, more specifically, on the eastern edge of the Great Slave Plain High Boreal Ecoregion (Ecosystem Classification Group, 2009). Jack pine (*Pinus banksiana*) and white spruce (*Picea glauca*) stands are common in this ecoregion. The study area is bounded to the east by Great Slave Lake (156 m a.s.l. — above sea level) and to the west by the base of a prominent 30 m high bedrock escarpment which rises from 200 m a.s.l. The underlying bedrock in the region is Cambrian- to Devonian-age dolomite, limestone, and sandstone (Ecosystem Classification Group, 2009). The upland terrain above the escarpment includes numerous marl lakes, wetlands, and pine forests characteristic of the ecoregion (Ecosystem Classification Group, 2009). Surficial materials include till and glaciolacustrine sediments. Till blankets consist of poorly sorted silt to gravel diamicton, typically more than 2 m thick (Stevens et al., 2017). The upland area is also covered by littoral and nearshore glaciolacustrine sediments composed of fine sand and silt, and ridged glaciolacustrine sandy gravel derived from reworked sediments associated

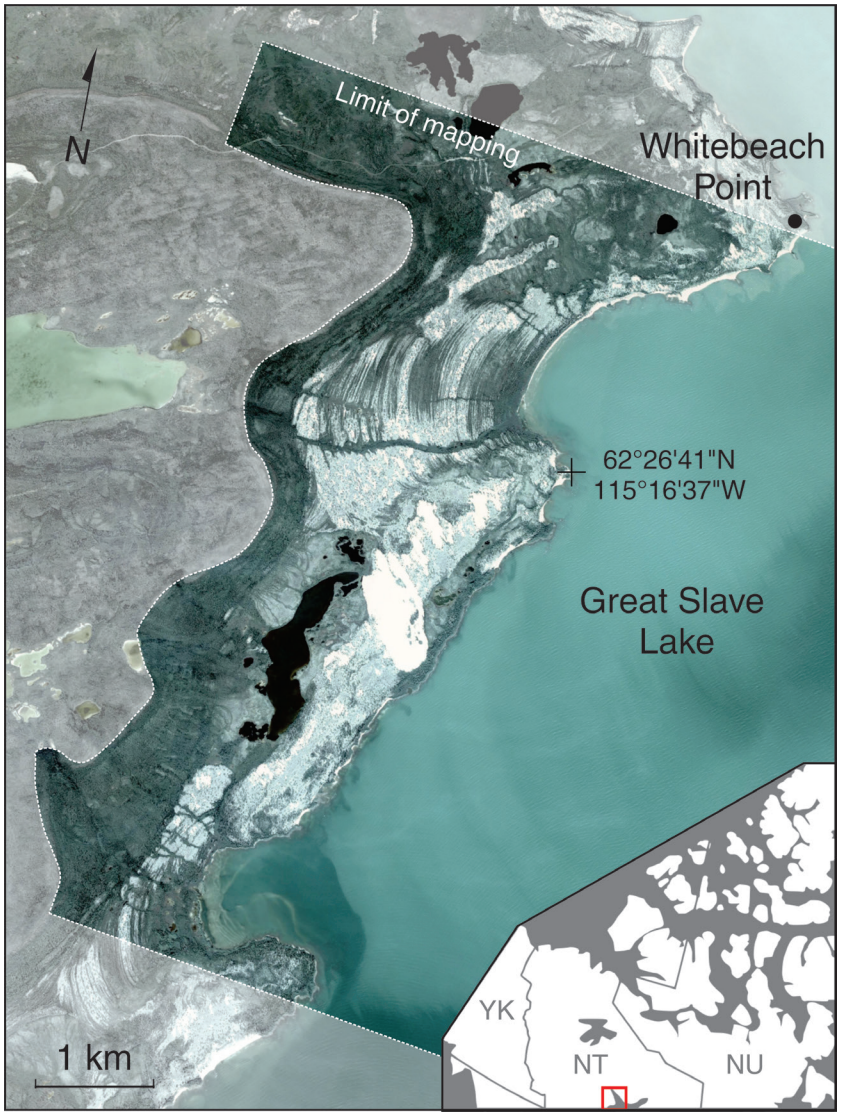

Figure 1. Extent of the mapped study area near Whitebeach Point, Northwest Territories. (Imagery from Google Earth: https://earth.google.com/web/)

with Glacial Lake McConnell and ancestral Great Slave Lake (Stevens et al., 2017). The sediment cover includes well defined beach ridges and terrace scarps, and small areas of bedrock (Stevens et al., 2017).

The study area and surrounding lowland terrain between Great Slave Lake and the limestone escarpment could be considered a unique lowland subclass of the Great Slave Plain High Boreal Ecoregion. The area is a gently sloping plain with a variable thickness of sediments overlying bedrock. The surficial cover includes extensive glaciolacustrine nearshore, littoral, and beach sediments, with overlying eolian sands in some areas. Vegetation includes jack pine, spruce, and birch forests, and isolated peatlands found surrounding shallow ponds and in low-lying areas.

The region has a subarctic continental climate, characterized by cold winters, warm summers, and a mean annual air temperature (1981–2010) of –4.1°C at Yellowknife, the nearest meteorological station, about 47 km to the east (Environment Canada, 2017). The study area is within the discontinuous permafrost zone (Heginbottom et al., 1995). Permafrost occurs in the region beneath peatlands and some forests growing on fine-grained lacustrine and glaciolacustrine deposits, but is absent in coarse-grained deposits and exposed bedrock (Karunaratne et al., 2008; Morse et al., 2016b). Permafrost is currently degrading in response to present climatic conditions (Morse et al., 2016b).

The area was glaciated until about 13.0 ka cal. BP (Dyke et al., 2003), and subsequently inundated by Glacial Lake McConnell (Smith, 1994). Prior to 6.0 ka cal. BP, exposed terrain north of Great Slave Lake was dominated by tundra, shrub tundra, and taiga (Huang et al., 2004), suggesting that a cooler climate prevailed than at present. Between 6.0 and 3.5 ka cal. BP, the treeline migrated north of its current position (MacDonald et al., 1993; Moser and MacDonald, 1990),

but the climate subsequently cooled after about 3.0 ka cal. BP (Huang et al., 2004). Though the regional climate has varied over the Holocene, the study area has likely remained within boreal or taiga forest (Dyke, 2005).

Whitebeach Point is a popular camping destination for boaters on Great Slave Lake (Northwest Territories Tourism, 2018). The area is also within the range of the Mackenzie wood bison (*Bison bison athabascae*) population, which is listed as a species of special concern by the Committee on the Status of Endangered Wildlife in Canada (COSEWIC) (Government of Canada, 2018). The area also lies just inside the southern boundary of Dınàgà Wek'èhodì, a 790 km^2 area of the north arm of Great Slave Lake considered an important area for migrating birds, and habitat for other birds, fish and wildlife. The area is of cultural importance and has been identified as a candidate protected area by the Tłıchǫ Government (DWWG, 2016).

Resource potential

There is a growing global demand for sand and gravel, mainly for use in concrete for building construction (Schandl et al., 2016), and also for high-grade silica sand used in hydraulic fracturing (i.e. 'fracking'). The demand for fracking sand has been spurred by a recent expansion in unconventional oil and gas production (Benson and Wilson, 2015). The sand is added to fracking fluids injected into oil and gas wells, where it serves to keep fractures open, allowing improved hydrocarbon extraction (Benson and Wilson, 2015). Most of the sand used in Canada originates in the Great Lakes region of Wisconsin (Snyder, 2017). However, local supply is preferable due to the added cost of transporting material by road and rail. High-grade silica sand is relatively uncommon in Canada, as much of the surficial sands are derived from glacial outwash, which tends to be mineralogically immature and contain carbonates, feldspars, and micaceous minerals. However, the eolian sands along the western shore of Great Slave Lake are silica-rich and present a potential high-grade resource for use in hydraulic fracturing.

METHODS

Mapping

High-resolution airborne lidar (light detection and ranging) and optical data were collected for a 156.7 km^2 area on August 3, 2013. The average flight height was 600 m above ground level at a speed of 240 km h^{-1}. A MATRIX system with a RIEGL Q560 laser was used, with a pulse rate of 137 kHz, resulting in a computed laser-point spacing of 0.71 m and average point density of 2.0 m^{-2}. Elevation data were georeferenced to the UTM Zone 11 map projection and the NAD83 (CSRS) horizontal datum, and to the CGVD28 vertical datum using the CGG2000 geoid with the HT 2.0 height transformation model. From this, a bare-earth digital elevation model (DEM) was compiled. The DEM and orthophotos were used to interpret surficial geology and geomorphic features (e.g. former shorelines, active sand dunes and sheets) and reconstruct the Holocene coastal evolution. Ground truthing was conducted during field visits between 2012 and 2017 (Wolfe et al., 2018).

Optical and radiocarbon dating

Seven optical dates from sand samples collected between 0.5 and 21.5 m above the present level of Great Slave Lake are available from the study site (Table 1). Three littoral sand samples were considered appropriate for deriving a lake-level regression curve, while eolian-sand and sand-wedge samples provide information on the timing of geomorphic processes active at the site. The littoral samples from the site imply lake-level regression of about 2.3 mm a^{-1} between ca. 7.0 ka and the present, obtained by joining the uppermost and lowermost data points with a straight line (Wolfe et al., 2018). This is similar to the rate of 2 mm a^{-1} reported by Vanderburgh and Smith (1988, Fig. 16) for the same time period from radiocarbon dates of samples from the Slave River delta. The rate is higher earlier in the Holocene, and

Table 1. Optical dates from sand at the study site (Wolfe et al., 2018). OSL = optically stimulated luminescence.

Sample	ID	Lat.	Long.	Elev. (m)	Depth (m)	Material	OSL age (years) (±1σ)
SAW12-02	1	62.42606	115.29675	0.5	0.50	Littoral sand	972 ± 82
SAW12-03	2	62.44436	115.30260	12.0	0.75	Littoral sand	5060 ± 560
SAW12-22	3	62.43256	115.29683	14.5	0.60	Littoral sand	7130 ± 530
SAW12-01	4	62.44406	115.31911	21.5	1.50	Eolian sand	5940 ± 670
SAW12-20	5	62.42811	115.29599	7.0	0.80	Eolian sand	2700 ± 390
SAW12-21	6	62.42811	115.29599	7.0	0.80	Sand wedge	2630 ± 200
SAW12-23	7	62.43256	115.29683	14.5	0.60	Sand wedge	1660 ± 180

the curve for the study area was extended based on dates collected above 170 m by Vanderburgh and Smith (1988) and Smith (1994) (Fig. 2).

Four radiocarbon dates are available from the site (Table 2). Three charcoal samples are from an excavation at a sand wedge, and the fourth is a basal peat sample from a peatland near the large lake at the site (Fig. 1). The samples underwent accelerator mass spectrometry (AMS) ^{14}C dating at the A.E. Lalonde AMS Laboratory, Ottawa, Canada. Complete background data related to the optical and radiocarbon dating for samples in tables 1 and 2 are found in Wolfe et al. (2018).

RESULTS

Surficial geology and geomorphology

Figure 3a depicts the present-day surficial geology and geomorphology of the study area interpreted from airphoto and lidar data and field observations. The locations of dated samples are indicated, along with the ages obtained. The legend in Figure 3a describes the features and sediments identified in the nearshore area below the escarpment. The landscape is a complex mosaic of Holocene sediments and landforms (Fig. 3a, 4, 5). The escarpment slope is covered by coarse colluvial material, occupying about 5% of the mapped area (Fig. 3a, 4a).

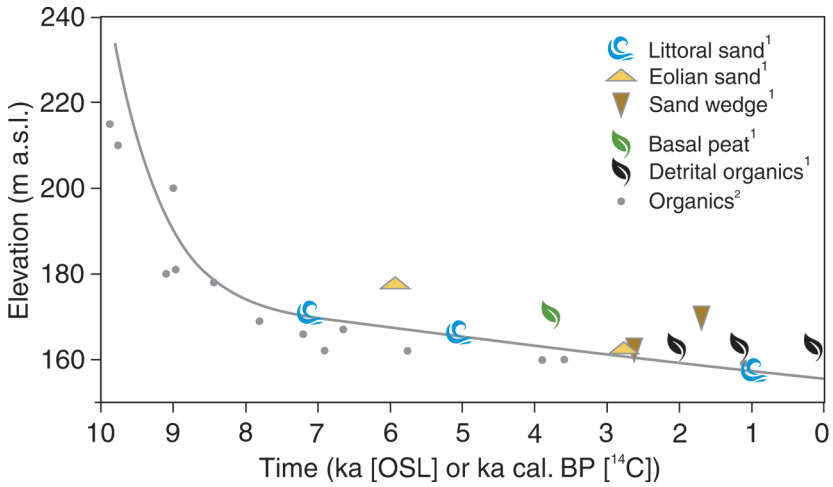

Figure 2. Optically-stimulated-luminescence (OSL) and calibrated-radiocarbon (^{14}C) dates for sand and organic samples, respectively. The estimated lake-level regression curve runs through the upper- and lowermost littoral-sand sample dates, and was fitted by hand through the data points at higher elevations. The superscript [1] denotes dates from Wolfe et al. (2018) for samples collected from the study site (Fig. 1). The superscript [2] indicates radiocarbon dates reported in Vanderburgh and Smith (1988) and Smith (1994) for samples from the Peace and Slave river deltas. For clarity, error bars are not shown but are reported in tables 1 and 2 for samples from Wolfe et al. (2018).

Table 2. Accelerator mass spectrometry (AMS) ^{14}C ages (Wolfe et al., 2018). Calibrations were performed using OxCal v4.2.4 (Bronk Ramsey, 2009) and the IntCal13 calibration curve (Reimer et al., 2013). Calibrated ages are reported in the results. Elevation is reported above the level of Great Slave Lake.

Sample	ID	Lat.	Long.	Elev. (m)	Depth (m)	Material	Pre-treatment	^{14}C years BP (±1σ)	Cal. years BP (±2σ)
UOC-0931	8	62.42811	115.29599	+7	0.20	Charcoal (composite)	None	101 ± 24	264-23
UOC-0932	9	62.42811	115.29599	+7	0.60	Charcoal (composite)	None	2071 ± 25	2124-1951
UOC-0933	10	62.42811	115.29599	+7	0.10	Charcoal (single)	Acid-Alkali-Acid	1241 ± 46	1277-1065
UOC-2619	11	62.42854	115.30344	+14.5	0.90	Bulk peat	Acid-Alkali-Acid	3513 ± 24	3850-3700

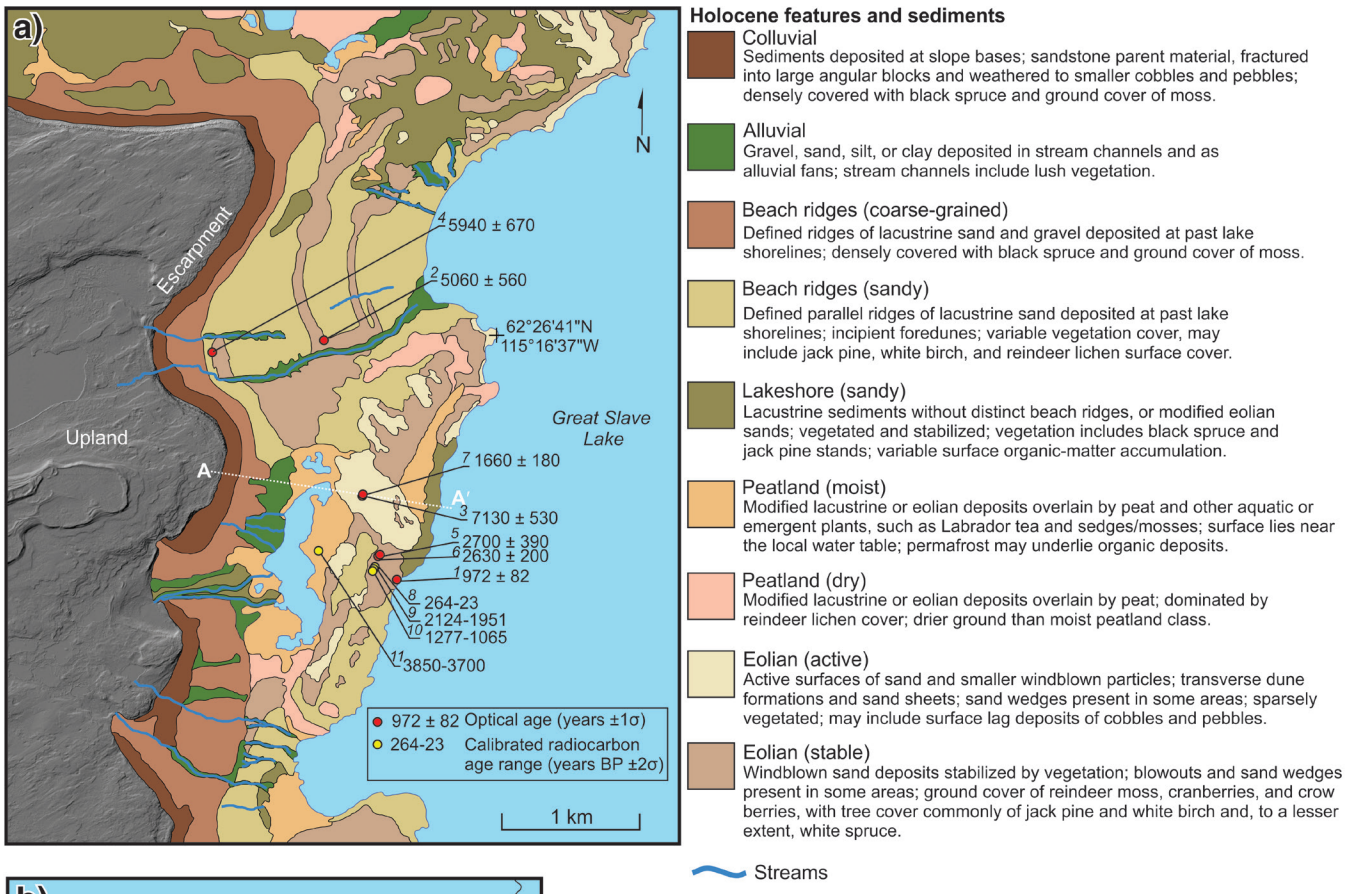

Figure 3. a) Present-day surficial geology and geomorphology of the study area, with locations of dated samples. The modern lake level is at 156 m a.s.l. **b)** Interpreted shoreline position at ca. 9 5 ka. MLL = modern lake level.

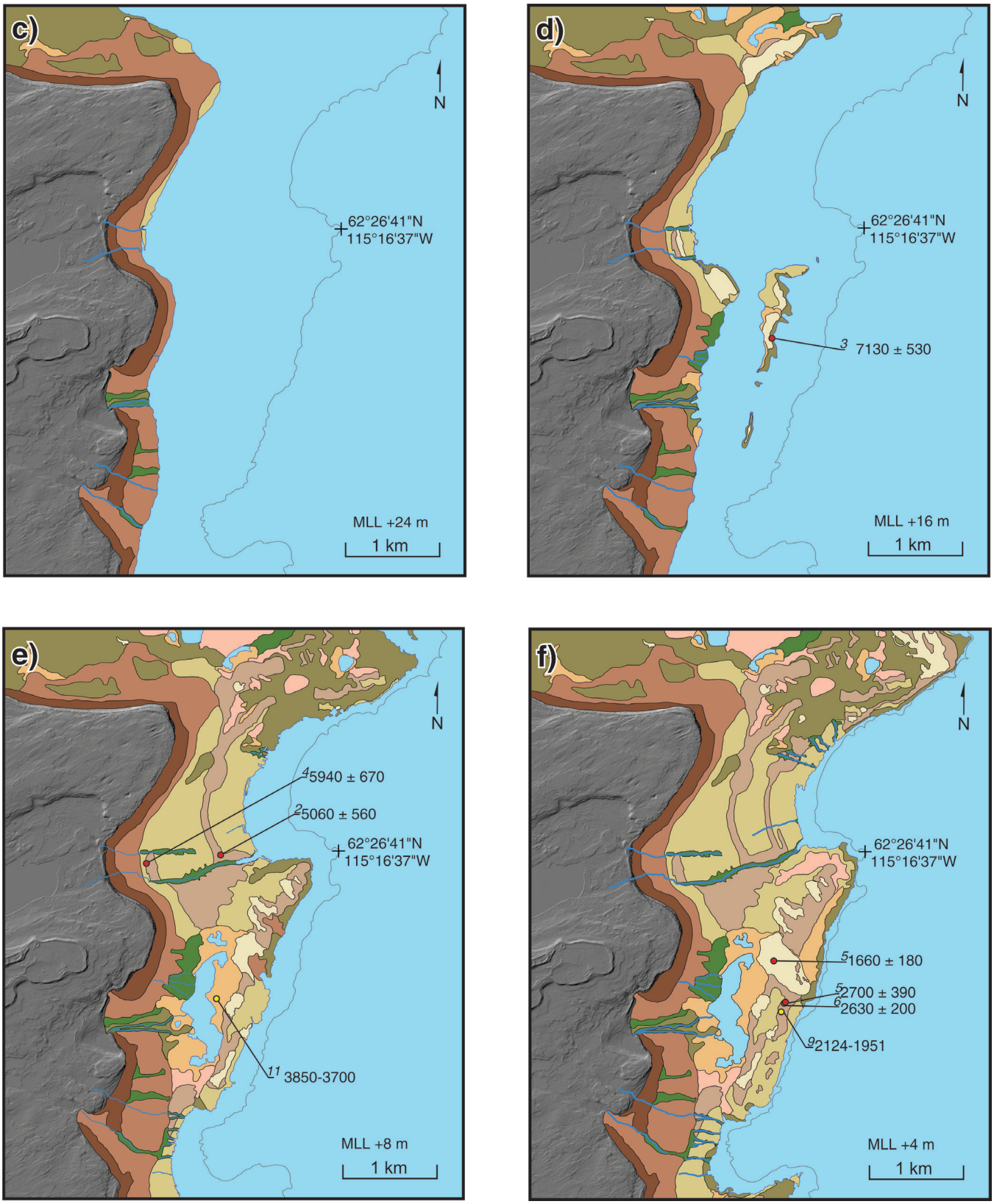

Figure 3. (cont.) c) Interpreted surficial geology, geomorphology, and shoreline position at ca. 8.6 ka. **d)** Interpreted surficial geology, geomorphology, and shoreline position at ca. 7.2 ka, with relevant dating control. **e)** Interpreted surficial geology, geomorphology, and shoreline position at ca. 3.5 ka, with relevant dating control. **f)** Interpreted surficial geology, geomorphology, and shoreline position at ca. 1.7 ka, with relevant dating control. MLL = modern lake level.

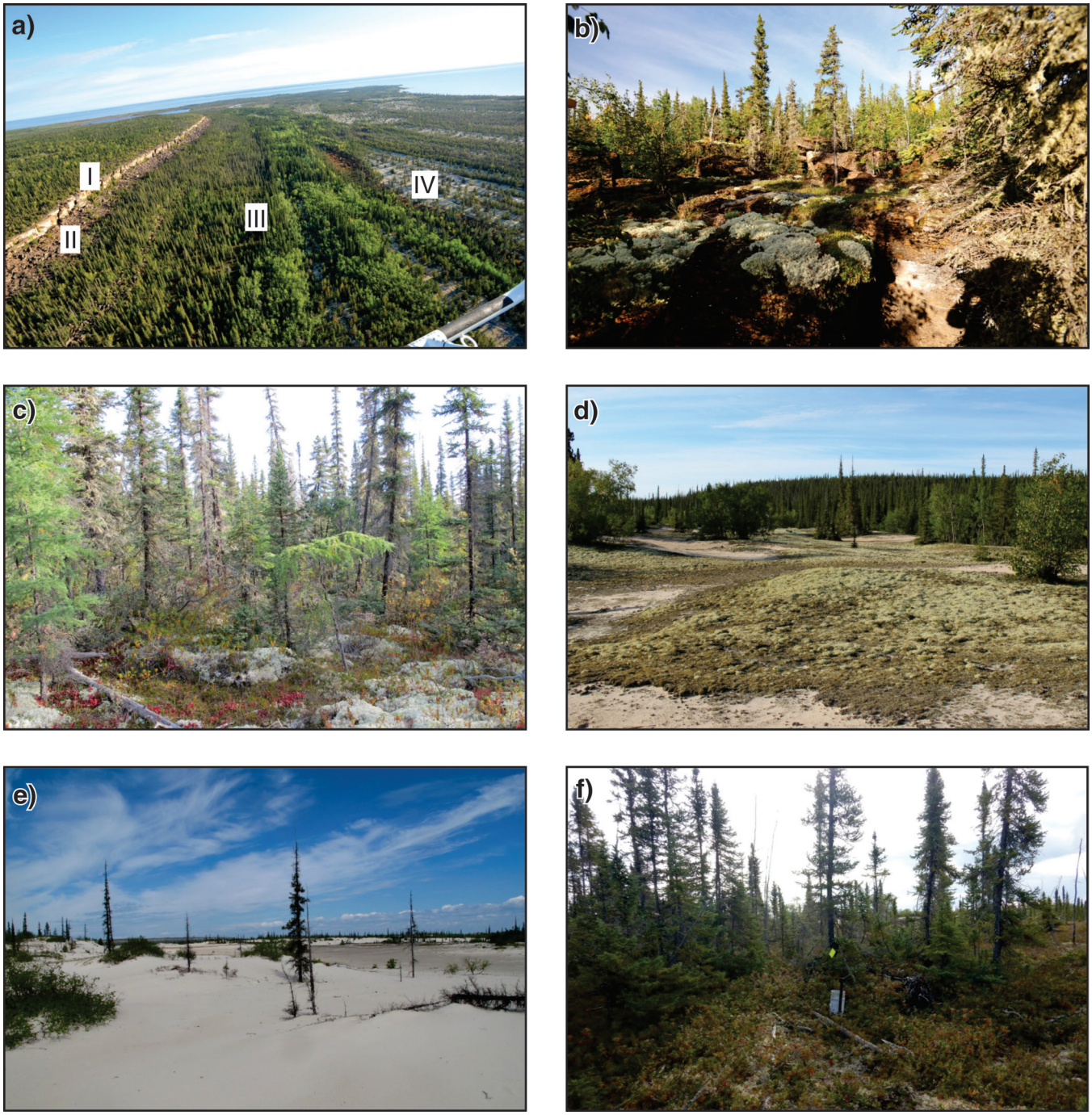

Figure 4. a) View of study area looking northward and including (I) bedrock escarpment, (II) colluvium, (III) coarse-grained beach ridges, and (IV) sandy beach ridges with incipient foredunes. Photograph by S. Schwarz. NRCan photo 2019-177 **b**) Forest and ground cover on the colluvium slope. Photograph by S. Schwarz. NRCan photo 2019-178 **c)** Black spruce forest and ground cover on coarse-grained beach ridges. Photograph by S.A. Wolfe. NRCan photo 2019-179 **d)** Ground cover and trees on sandy beach ridges with forested coarse-grained beach ridges in background. Photograph by S.A. Wolfe. NRCan photo 2019-180 **e)** Active eolian sand area with sand dune in foreground and erosional surface in background. Photograph by S.A. Wolfe. NRCan photo 2019-181 **f)** Moist peatland area with thick ground cover and black spruce woodland. Photograph by W. Sladen. NRCan photo 2019-182

The colluvium consists of weathered parent sedimentary bedrock dislodged from the escarpment. Vegetation cover near the escarpment is sparse, as the area consists primarily of large blocks and boulders (Fig. 4a), whereas the lower slope is covered by black spruce (*Picea mariana*) and white birch (*Betula papyrifera*) with an understory of lichen, mosses, and herbaceous shrubs, and areas of exposed rock (Fig. 4b).

Extensive coarse-grained beach ridges and sandy foredune complexes are preserved inland from embayments, marking the recession of former lake shorelines (Fig. 1, 3a, 4a). Coarse-grained beach ridges occupy about 12% of the total mapped area; they consist predominantly of gravel and coarse sand and occur adjacent to the colluvium, marking wave-cut terraces along the base of the escarpment. They are forested with black spruce and birch, with a ground cover of lichen, moss, willows, Labrador tea (*Rhododendron tomentosum*), and other herbaceous shrubs (Fig. 4c). The ground in these areas is generally shaded and moist. Sandy beach ridges that include well defined incipient foredunes are more extensive, covering about 38% of the mapped area (Fig. 3a, 4a). These sandy ridges extend from the lakeshore to about 2 km inland, up to about 183 m elevation, and are typically vegetated by jack pine, white birch, and an understory of reindeer lichen (*Cladonia rangiferina*), with small pockets of black spruce and Labrador tea. Some more open areas lack tree cover, possibly due to past forest fires (Fig. 4d).

Active and stabilized eolian surfaces are abundant (Fig. 3a). Active features cover 4% of the mapped area and include sand sheets, transverse dunes, and some blowouts (Fig. 4e). The largest active dune is about 1000 m long by 400 m wide. Stabilized eolian surfaces with vegetation cover make up about 12% of the mapped area. Vegetation cover in these areas includes a ground cover of reindeer lichen, cranberry (*Vaccinium vitis-idaea*) and crowberry (*Empetrum nigrum*), with tree cover commonly of jack pine, white birch, and some white spruce. Sand wedges, which form due to thermal contraction cracking of the ground in winter and subsequent infilling, are present in some areas within active and stable eolian deposits with little snow cover in winter (Wolfe et al., 2018). Erosion has removed eolian sand in some locations, forming cobble and pebble lag deposits (Wolfe et al., 2018).

Other sandy terrain lacking distinct beach ridges or obvious eolian deposits is distributed throughout the area and is interpreted as a lacustrine lakeshore unit. These areas occupy about 13% of the mapped area. Vegetation cover is similar to that of stabilized eolian terrain, but may be more dense and include greater surface organic accumulation.

Peatlands overlie eolian or lacustrine sediments in some areas and can be subdivided based on prevailing moisture conditions. Moist peatlands, covering about 6% of the study area, lie near the local water table. They are distributed mainly around the lake in the southern central part of the study area, and near the present shoreline of Great Slave Lake. Moist peatlands host aquatic or emergent plants and Labrador tea, sedges, and mosses (Fig. 4f). Drier peatlands (4% coverage) are found mainly in the north of the study area adjacent to small lakes. The surface cover is dominated by reindeer lichen. A series of small streams flow from the escarpment to Great Slave Lake, depositing sediments in narrow beds and in alluvial fans (Fig. 3a).

Several small lakes and ponds lie within the study area and are surrounded by peatlands. The largest lake occurs in the southern part of the study area and is over a kilometre long and several hundred metres wide. Is it fed by several streams flowing off the escarpment, with small alluvial fan-deltas entering the lake. Water bodies occupy about 2% of the mapped study area (excluding Great Slave Lake).

Fire appears to have partly controlled the landscape development in the study area, as some terrain units are clear of treed vegetation. South of the large active dune, tree-ring analyses of re-sprouted white birch trees suggest that the stabilized eolian terrain was burned approximately 80 years ago (Wolfe et al., 2018). It is possible that active eolian terrain represents areas that have become wind-modified following forest fires.

Figure 5 illustrates a cross-sectional topographic profile from the escarpment to Great Slave Lake along the transect A-A' identified in Figure 3a. The steep topographic gradient is evident between the escarpment head at about 225 m and the lower-elevation surficial units at about 175 m. This likely exerts strong topographic control on surface and groundwater flow across the study area. The topographic gradient is gentle between the base of the escarpment and the modern shoreline across the sandy-beach deposits and eolian sediments.

INTERPRETATION AND DISCUSSION

Holocene lake-level regression and shoreline reconstruction

Circa 9.5 ka

Prior to ca. 9.5 ka, the elevation of Glacial Lake McConnell was about 290–300 m a.s.l., covering the uplands above the escarpment (200–210 m a.s.l.) in the study area. As the water level fell, till was reworked and deposited as glaciolacustrine sediments, leaving a series of beach crests in some upland areas (Stevens et al., 2017). By ca. 9.5 ka, the lake level had receded to 216 m a.s.l., about 60 m above the modern level, and the shoreline rested along the escarpment (Fig. 3b). At this time, none of the mapped surficial sediments existing today and described above had been deposited or terrestrially exposed, and the shoreline likely consisted of undifferentiated glacial sediments and bedrock.

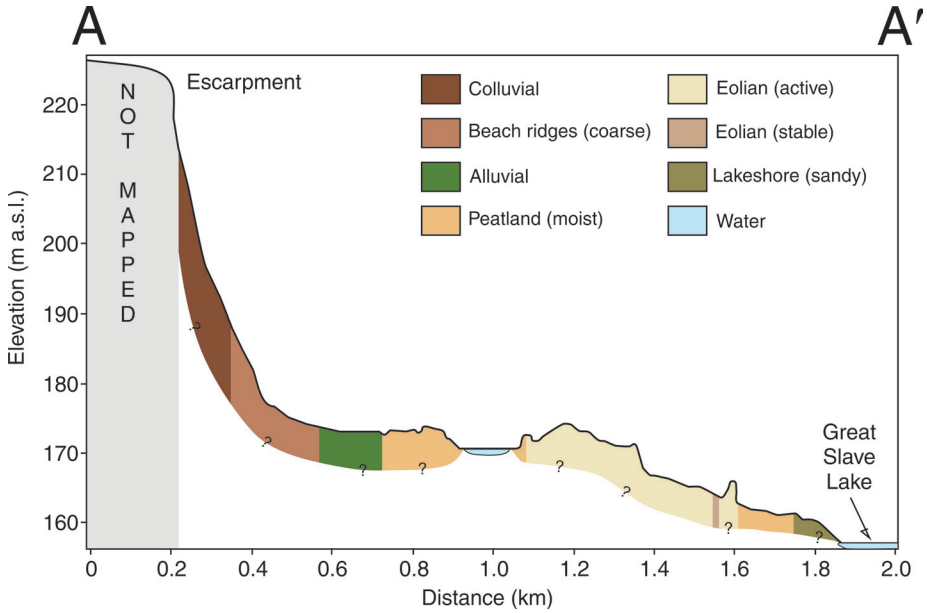

Figure 5. Topographic profile from the escarpment to the shore of Great Slave Lake along transect A-A' in Figure 3a. The thicknesses of the surficial units are unknown. Vertical exaggeration of the elevation profile is ~17x.

Circa 9.5 ka to 8.6 ka

By ca. 9.3 ka (8300 ^{14}C years BP), ongoing isostatic rebound had caused regression of Glacial Lake McConnell and its division into the Great Slave and Athabasca basins (Smith, 1994). Continued regression of ancestral Great Slave Lake between ca. 9.5 and 8.6 ka progressively exposed the slope beneath the escarpment in the study area. Colluviation began moving weathered material downslope (Fig. 3c). Concurrently, coarse gravels, cobbles, and sand derived from glaciofluvial sediments were reworked and deposited as beach ridges (Stevens et al., 2017) (Fig. 3c). Streams draining the upland crosscut the colluvial and beach sediments, eroding and transporting material to the lake (Fig. 3c).

Circa 8.6 to 7.2 ka

By ca. 7.2 ka, continued regression of ancestral Great Slave Lake exposed a swath of sandy lacustrine sediments about 0.5 km wide and trending north-south, parallel to the escarpment (Fig. 3d). Sandy beach ridges and foredunes began to form in and north of the embayment (Fig. 3d). The foredunes are similar to those reported from other subarctic environments with emerging coastlines (e.g. Ruz and Allard, 1994). Unvegetated lakeshore deposits likely provided material for eolian mobilization and the initiation of sand sheets and dunes (e.g. Koster, 1988; Wolfe et al., 2011). Offshore, a small ridge emerged as an island. The topography of this feature may be controlled by underlying bedrock. Littoral sands from this location are dated at ca. 7.1 ka (Table 1, ID 3). The island likely protected the adjacent shoreline from wave action and wind, preventing the continued formation of distinct beach ridges and foredunes like those present just north in the embayment (Fig. 3a, d). During this period, the rate of lake-level regression decreased significantly.

Circa 7.2 to 3.5 ka

The interpreted rate of lake-level regression from ca. 7.2 to 3.5 ka decreased to about 2.3 mm a^{-1} (Fig. 2). The small offshore island likely joined the mainland soon after ca. 7.2 ka, forming a lake in the backshore basin over a kilometre in length (Fig. 3e). The lake was likely supplied with water by streams flowing off the escarpment as it is today, forming a sandy alluvial fan-delta on the lake's western shore. An optical date from sand of ca. 5.9 ka (Table 1, ID 4) indicates the minimum age of eolian sedimentation near the head of the large embayment (Fig. 3e). Dating of littoral sand indicates that the shoreline had regressed several hundred metres by ca. 5.0 ka (Table 1, ID 2). A date from basal peat near the lake indicates organic accumulation had commenced by about 3.8 ka (Table 2, ID 11). The peat at this location is about 1.0 m thick and underlain by sand (Wolfe et al., 2018). The implied rate of peat accumulation is thus about 0.26 cm a^{-1}. It is possible that by 3.5 ka, previously active sand surfaces had stabilized with vegetation. Fires, wind, and effective drainage in sandy areas without permafrost likely contributed to dry conditions that enhanced eolian activity.

Circa 3.5 to 1.7 ka

Between ca. 3.5 and 1.7 ka, slow shoreline regression continued. Several dated samples provide evidence of active geomorphic processes during this period (Fig. 3f). A sand sample dated at ca. 2.7 ka (Table 1, ID 5) indicates terrestrial emergence and eolian sedimentation in an aggrading sand sheet (Fig. 3f). At the same location, a sample from a sand wedge was dated at ca. 2.6 ka (Table 1, ID 6), indicating sand-wedge growth concurrent with aggradation of the host eolian sheet sands (Fig. 3f; Wolfe et al., 2018). Peat growth, and the associated establishment of permafrost, likely increased at this time to reach a late Holocene maximum due to climatic cooling (Huang et al., 2004).

Circa 1.7 ka to present

Continued lake-level regression exposed further ground and resulted in the present-day geomorphic setting (Fig. 3a). During this period, the shoreline position moved slowly, as indicated by an optical age from littoral sand of ca. 0.9 ka (Table 1, ID 1) near the present-day lakeshore (Fig. 3a).

Permafrost distribution and hydrology

Permafrost has aggraded since deglaciation and lake regression, but the lack of a long-term climatic record or reconstruction for the region makes it difficult to determine the past extent of permafrost in the mapped area. However, the widespread cover of sandy sediments, recent terrestrial emergence, and frequent fire regime in the northern boreal forest suggest that permafrost distribution has likely been limited in much of the study area during the Holocene. Figure 6 depicts an interpreted current distribution of permafrost informed by field observations and measured ground temperatures from Wolfe et al. (2018).

Permafrost is likely only widespread in areas where surface organic material is more than about 30 cm thick, primarily in the peatland surficial classes (Fig. 6). The presence of permafrost has been confirmed in the study area by field measurements from the peatland adjacent to the large lake (Wolfe et al., 2018). Active-layer thickness in the peatland is about 90 cm, and the permafrost is relatively warm, with ground temperatures at 1.00 m depth remaining above –3°C in winter (Wolfe et al., 2018). Discontinuous permafrost may underlie undifferentiated lakeshore sediments and coarse-grained beach ridges in well vegetated areas with substantial surface organic-matter accumulation. Most other terrain units, including stabilized eolian areas and colluvium, are likely underlain by seasonally frozen ground. However, some thin, isolated patches of permafrost may occur where vegetation is well established. It is possible that large blocks and cobbles in the colluvial deposits act to produce passive cooling from the free convection of air, resulting in isolated patches of permafrost (Bishop-Legowski, 2019; Juliussen and Humlum, 2008). Where it exists, permafrost is likely relatively thin, given the warm near-surface ground temperatures observed at the site. Permafrost is probably absent under all active eolian surfaces, as no frozen ground was encountered during augering at the site. Seasonal frost in these areas can penetrate to depths in excess of 4 m where the sandy terrain is well drained (Wolfe et al., 2018).

The significant topographic gradient between the top of the escarpment at 230 m and Great Slave Lake at 156 m, combined with the occurrence of discontinuous permafrost, likely exerts strong control on surface and groundwater hydrology in the study area. Figure 7 provides a conceptual depiction of surface and groundwater flow paths across the A-A' transect (*see* Figure 5). This should be considered a preliminary model and hypothetical, as field measurements of groundwater flow were not collected in this study. Hydrological investigations at the site will allow refinement and testing of the conceptual model.

Surface runoff into Great Slave Lake is evident from the many streams flowing eastward from the escarpment (Fig. 3a, 7). Snowmelt and rainfall are likely transmitted effectively to the subsurface in areas underlain by unfrozen sandy sediment. Such effective drainage is suggested by low gravimetric moisture contents (<5%) measured in near-surface sands at the site (Wolfe et al., 2018). On the escarpment slope, infiltration is likely facilitated in the blocky colluvial material and well fractured and porous sedimentary bedrock, where only isolated patches of permafrost may exist (Fig. 7). Permafrost in well vegetated areas will limit infiltration and obstruct the flow of groundwater, resulting in confinement within the thawed active layer and below the base of frozen ground at greater depth (Fig. 7). The water table in the active eolian surface to the east of the lake was encountered during augering at depths between 4.00 and 5.00 m (Wolfe et al., 2018). The depth of seasonal freezing may therefore reach the top of the groundwater table in some areas, where the saturated soil likely inhibits further penetration of the freezing front due to the high latent heat capacity. Changes in the distribution of seasonally frozen ground and permafrost due to climatic, ecological, or anthropogenic factors will likely have a significant effect on groundwater flow patterns and the water table in the study area.

Holocene landscape development and eolian processes

The study area, like the entire Great Slave Lake basin, has undergone Holocene lake-level regression due mainly to isostatic rebound since deglaciation. The estimated average rate of Late Holocene lake-level regression in the study area is about 2.3 mm a^{-1} (Fig. 2). This is comparable to the rate of 2.0 mm a^{-1} estimated for southern Great Slave Lake (Smith, 1994) but significantly less than the rate of 5 mm a^{-1} estimated near Yellowknife, to the east (Wolfe and Morse, 2017). These differences may be due to variation in glacial loading,

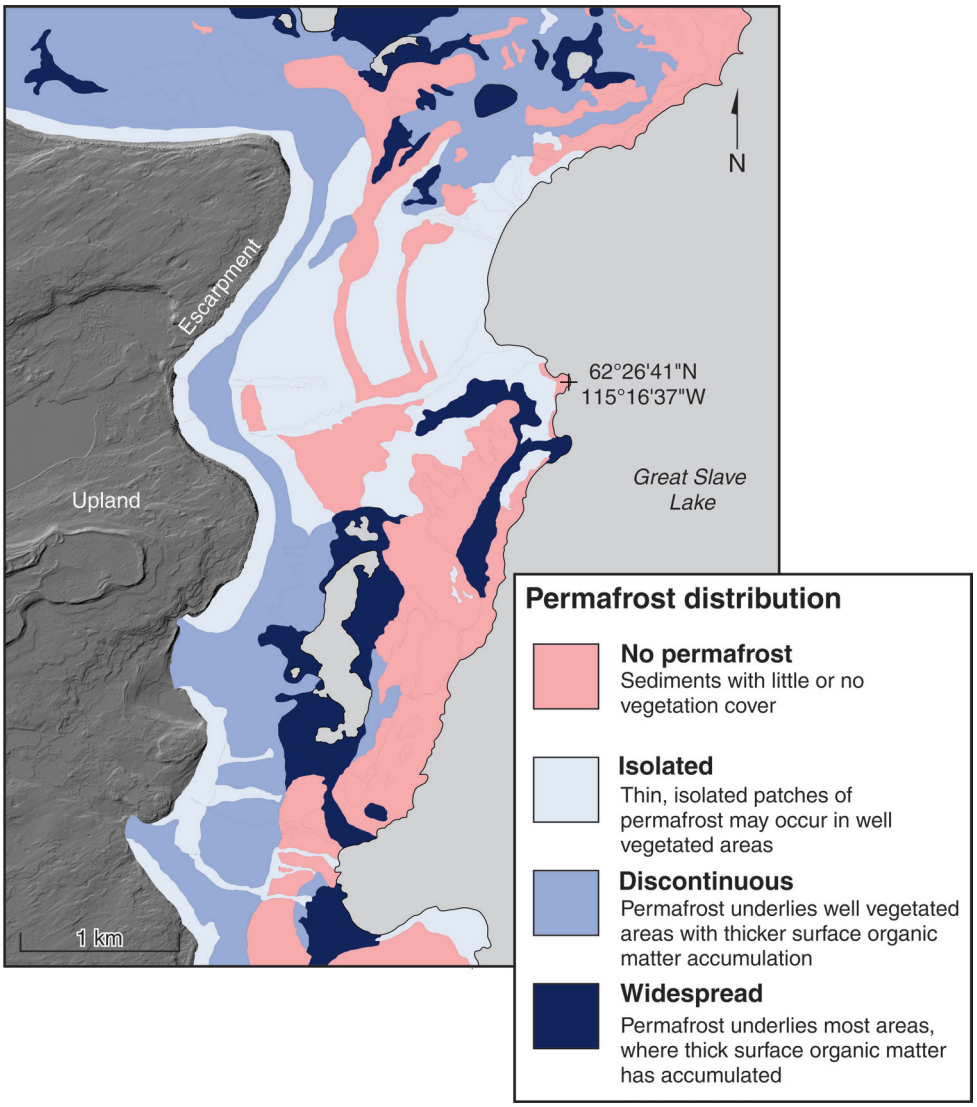

Figure 6. Permafrost distribution inferred from field measurements and extrapolated to the mapped surficial-geology units.

which generally increases eastward-northeastward, bedrock characteristics, and the specific configuration of the ice front during retreat. Though the rate of 5 mm a^{-1} near Yellowknife is higher than those for the study area and southern Great Slave Lake, models suggest that the Laurentide Ice Sheet was thicker in the vicinity of Yellowknife than at Whitebeach Point (Gowan et al., 2016; Tarasov et al., 2012). Further north, a rebound rate of 4 mm a^{-1} over the last 5 ka is estimated near Kugluktuk (D.E. Kerr, unpub. data, 2019), where rates of isostatic rebound over the past 10 ka BP are interpreted as similar to those near Yellowknife (e.g. Lemmen et al., 1994, Fig. 6).

Isostatic rebound has resulted in continually changing geomorphology and ecology in the study area and the Great Slave Lake basin over the last several thousand years. This is particularly evident in the low-relief areas at elevations between about 200 m and the modern Great Slave Lake level (156 m a.s.l.), which are commonly covered by glaciolacustrine and lacustrine sediments. The shoreline in the study area has prograded between 1.5 and 3 km over the last 9.5 ka, and glaciolacustrine and lacustrine deposits have been further modified by eolian processes (Fig. 3). Long-term eolian erosion and deposition have formed active and stabilized incipient shoreline foredunes, sand dunes, sand sheets, blowouts, coarse granular ripples and corridors, ventifacts (wind-abraded rocks), and "ghost" forests (wind-exhumed dead forests). In some areas, eolian erosion has removed finer-grained surficial sediments, leaving a coarse cobble and boulder lag near the ground surface, underlain by beach deposits and/or possibly till. In other areas, the wind-blown sand has accumulated as dunes over 8 m in height. These eolian sand surfaces promote thermal-contraction cracking and sand-wedge formation (Wolfe et al., 2018). Cracking is possible due to the absence of vegetation and associated snow cover, and the low moisture content of

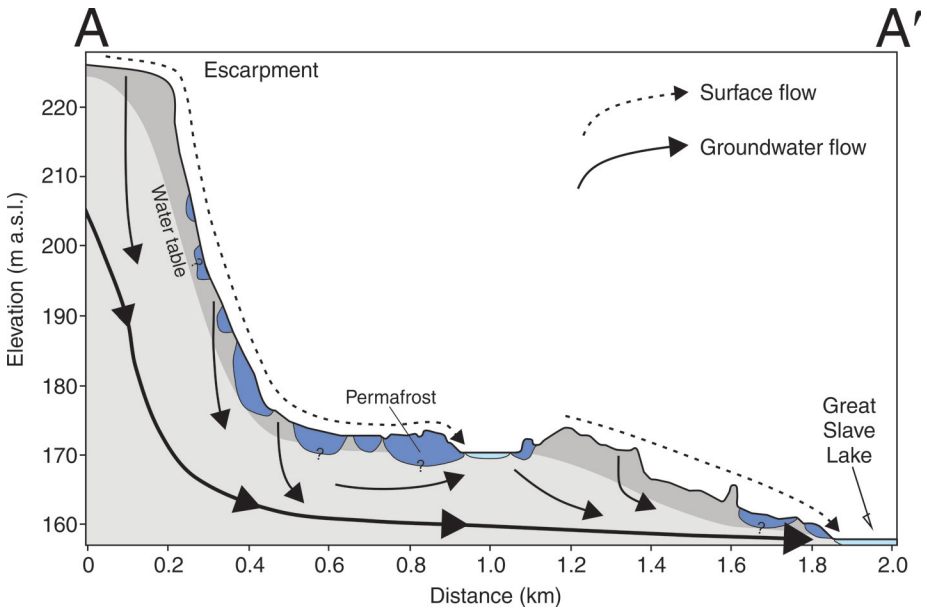

Figure 7. Conceptual diagram of surface and groundwater flow between the escarpment and Great Slave Lake along transect A-A'. The permafrost distribution and water-table configuration are interpreted, based on limited field data. Vertical exaggeration of the elevation profile is ~17x.

near-surface sands, which both contribute to very low winter ground temperatures. Sand wedges form in seasonally frozen eolian sediments at the site, but not in peatlands underlain by permafrost, where snow cover is thicker and winter ground temperatures are much higher.

CONCLUSIONS

This study adds to an understanding of terrestrial emergence and landscape development associated with the regression of glacial Lake McConnell and Great Slave Lake. It advances current understanding of the formation of Holocene silica-rich eolian sands on the shores of Great Slave Lake, which have environmental, cultural, and potential resource value. The study provides a surficial geological context for industry and decision-makers to aid regional infrastructure planning, mineral exploration, and land-use allocation in the area.

ACKNOWLEDGMENTS

This report was written during the senior author's term in Natural Resources Canada's Postdoctoral Research Program, and is a contribution to the Mackenzie project of the Geoscience for Energy and Minerals (GEM) program. Assistance with mapping and GIS analysis was provided by Samuel Jardine during a casual employment work term. Husky Energy is gratefully acknowledged for providing lidar data to the Geological Survey of Canada for analysis. Helpful discussions with Explor Silica and review comments provided by A. Châtenay improved the manuscript.

REFERENCES

Benson, M.E. and Wilson, A.B., 2015. Frac sand in the United States: a geological and industry overview; U.S. Geological Survey Open-File Report 2015-1107; U.S. Geological Survey, Reston, VA, 78 p.

Bishop-Legowski, S., 2019. Thermal regime of two talus slopes in northwestern Ontario; M.Sc. Thesis, Carleton University, Ottawa, Ontario, 192 p.

Bronk Ramsey, C., 2009. Bayesian analysis of radiocarbon dates; Radiocarbon, v. 51, p. 337–360. https://doi.org/10.1017/S0033822200033865

Brown, R.J., 1966. Relation between mean annual air and ground temperatures in the permafrost regions of Canada; *in* Proceedings of the 1st International Permafrost Conference, National Research Council Publications, Ottawa, Ontario, p. 241–247.

Brown, R.J., 1973. Influence of climatic and terrain factors on ground temperatures at three locations in the permafrost region of Canada; *in* Proceedings of the 2nd International Conference on Permafrost, North American Contribution, National Academy of Science, Washington, D.C., p. 27–34.

Craig, B.G., 1965. Glacial Lake McConnell and the surficial geology of parts of Slave River and Redstone River map areas, District of Mackenzie; Geological Survey of Canada, Bulletin 122, 44 p. https://doi.org/10.4095/100639

Duk-Rodkin, A. and Lemmen, D.S., 2000. Glacial history of the Mackenzie region; *in* The physical environment of the Mackenzie Valley, Northwest Territories: a base line for the assessment of environmental change, (ed.) L.D. Dyke and G. Brooks; Geological Survey of Canada, Bulletin 547, p. 11–20. https://doi.org/10.4095/211903

DWWG, 2016. Working Group Report prepared by the Dinàgà Wek'èhodì Candidate Protected Area Working Group < www.enr.gov.nt.ca/sites/enr/files/dinaga_wek_ehodi_final_draft_working_group_report_31_march_2016.pdf > [accessed November 16, 2018]

Dyke, A.S., 2005. Late quaternary vegetation history of northern North America based on pollen, macrofossil, and faunal remains; Géographie physique et Quaternaire, v. 59, p. 211. https://doi.org/10.7202/014755ar

Dyke, A.S., Moore, A., and Robertson, L., 2003. Deglaciation of North America; Geological Survey of Canada, Open File 1574, 1 .zip file. https://doi.org/10.4095/214399

Ecosystem Classification Group, 2009. Ecological regions of the Northwest Territories – Taiga Plains; Department of Environment and Natural Resources, Government of the Northwest Territories, Yellowknife, Northwest Territories, 173 p. (revised edition)

Ednie, M., Kerr, D.E., Olthof, I., Wolfe, S.A., and Eagles, S., 2014. Predictive surficial geology derived from LANDSAT 7, Marian River, NTS 85-N, Northwest Territories; Geological Survey of Canada, Open File 7543, 21 p. https://doi.org/10.4095/294923

Environment Canada, 2017. Historical climate data. <http://climate.weather.gc.ca/> [accessed May 16, 2017]

Government of Canada, 2018. A to Z Species Index. Species at Risk Public Registry. <http://www.registrelep-sararegistry.gc.ca/sar/index/default_e.cfm> [accessed July 13, 2018]

Gowan, E.J., Tregoning, P., Purcell, A., Montillet, J.-P., and McClusky, S., 2016. A model of the western Laurentide Ice Sheet, using observations of glacial isostatic adjustment; Quaternary Science Reviews, v. 139, p. 1–16. https://doi.org/10.1016/j.quascirev.2016.03.003

Heginbottom, J.A., Dubreuil, M.-A., and Harker, P.A.C., 1995. Canada — Permafrost; Natural Resources Canada, National Atlas of Canada, 5th ed., MCR 4177, scale 1:7 500 000. https://doi.org/10.4095/205314

Huang, C.C., MacDonald, G.M., and Cwynar, L., 2004. Holocene landscape development and climatic change in the low arctic, Northwest Territories, Canada; Palaeogeography, Palaeoclimatology, Palaeoecology, v. 205, p. 221–234. https://doi.org/10.1016/j.palaeo.2003.12.009

Juliussen, H. and Humlum, O., 2008. Thermal regime of openwork block fields on the mountains Elgåhogna and Sølen, central-eastern Norway; Permafrost and Periglacial Processes, v. 19, p. 1–18. https://doi.org/10.1002/ppp.607

Karunaratne, K.C., Kokelj, S.V., and Burn, C.R., 2008. Near-surface permafrost conditions near Yellowknife, Northwest Territories, Canada; *in* Proceedings of the 9th International Conference on Permafrost, University of Alaska, Fairbanks, Alaska, p. 907–912.

Kerr, D.E. and O'Neill, H.B., 2017. Reconnaissance surficial geology, Indin Lake, Northwest Territories, NTS 86-B; Geological Survey of Canada, Canadian Geoscience Map 334, preliminary edition, scale 1:125 000. https://doi.org/10.4095/306108

Kerr, D.E. and O'Neill, H.B., 2018a. Reconnaissance surficial geology, Rivière Grandin, Northwest Territories, NTS 86-D; Geological Survey of Canada, Canadian Geoscience Map 361, preliminary edition, scale 1:125 000. https://doi.org/10.4095/308479

Kerr, D.E. and O'Neill, H.B., 2018b. Reconnaissance surficial geology, Hardisty Lake, Northwest Territories, NTS 86-C; Geological Survey of Canada, Canadian Geoscience Map 337, preliminary edition, scale 1:125 000. https://doi.org/10.4095/306290

Kerr, D.E., Knight, R.D., Sharpe, D.R., Cummings, D.I., and Kjarsgaard, B.A., 2014. Surficial geology, Snowdrift, Northwest Territories, NTS 75-L; Geological Survey of Canada, Canadian Geoscience Map 137, 2nd preliminary edition, scale 1:125 000. https://doi.org/10.4095/295496

Kerr, D.E., Morse, P.D., and Wolfe, S.A., 2016. Reconnaissance surficial geology, Rae, Northwest Territories, NTS 85-K; Geological Survey of Canada, Canadian Geoscience Map 290, preliminary edition, scale 1:125 000. https://doi.org/10.4095/298838

Kerr, D.E., Morse, P.D., and Wolfe, S.A., 2017. Reconnaissance surficial geology, Lac la Martre, Northwest Territories, NTS 85-M; Geological Survey of Canada, Canadian Geoscience Map 306, 2nd preliminary edition, scale 1:125 000. https://doi.org/10.4095/304282

Koster, E.A., 1988. Ancient and modern cold-climate aeolian sand deposition: A review; Journal of Quaternary Science, v. 3, p. 69–83. https://doi.org/10.1002/jqs.3390030109

Lemmen, D.S., 1990. Surficial materials associated with glacial Lake Mcconnell, southern District of Mackenzie; *in* Current Research, Part D; Geological Survey of Canada, Paper 90–1D, p. 79-83. https://doi.org/10.4095/131342

Lemmen, D.S., Duk-Rodkin, A., and Bednarski, J.M., 1994. Late glacial drainage systems along the northwestern margin of the Laurentide Ice Sheet; Quaternary Science Reviews, v. 13, p. 805–828. https://doi.org/10.1016/0277-3791(94)90003-5

MacDonald, G.M., Edwards, T.W.D., Moser, K.A., Pienitz, R., and Smol, J.P., 1993. Rapid response of treeline vegetation and lakes to past climate warming; Nature, v. 361, p. 243–246. https://doi.org/10.1038/361243a0

Morse, P.D., Kerr, D.E., Wolfe, S.A., and Olthof, I., 2016a. Predictive surficial geology, Wecho River, Northwest Territories, NTS 85-O; Geological Survey of Canada, Canadian Geoscience Map 277, preliminary edition, scale 1:125 000. https://doi.org/10.4095/298686

Morse, P.D., Wolfe, S.A., Kokelj, S.V., and Gaanderse, A.J.R., 2016b. The occurrence and thermal disequilibrium state of permafrost in forest ecotopes of the Great Slave Region, Northwest Territories, Canada; Permafrost and Periglacial Processes, v. 27, p. 145–162. https://doi.org/10.1002/ppp.1858

Moser, K.A. and MacDonald, G.M., 1990. Holocene vegetation change at treeline north of Yellowknife, Northwest Territories, Canada; Quaternary Research, v. 34, p. 227–239. https://doi.org/10.1016/0033-5894(90)90033-H

Northwest Territories Tourism, 2018. Where to hit the beach — Spectacular Northwest Territories. <http://spectacularnwt.com/story/where-to-hit-beach> [accessed July 13, 2018].

Oviatt, N.M. and Paulen, R.C., 2013. Surficial geology, Breynat Point, Northwest Territories, NTS 85-B/15; Geological Survey of Canada, Canadian Geoscience Map 114, preliminary edition, scale 1:50 000. https://doi.org/10.4095/292247

Paulen, R.C., Smith, I.R., Day, S.J.A., Hagedorn, G.W., King, R.D., and Pyne, M.D., 2017. GEM2 Southern Mackenzie Surficial Activity 2017 report of activities: surficial geology and heavy mineral studies in southern Northwest Territories; Geological Survey of Canada, Open File 8322, 27 p. https://doi.org/10.4095/306090

Prest, V.K., Grant, D.R., and Rampton, V.N., 1968. Glacial map of Canada; Geological Survey of Canada, Map 1253A, scale 1:5 000 000. https://doi.org/10.4095/108979

Reimer, P.J., Bard, E., Bayliss, A., Beck, J.W., Blackwell, P.G., Ramsey, C.B., Buck, C.E., Cheng, H., Edwards, R.L., Friedrich, M., Grootes, P.M., Guilderson, T.P., Haflidason, H., Hajdas, I., Hatté, C., Heaton, T.J., Hoffmann, D.L., Hogg, A.G., Hughen, K.A., Kaiser, K.F., Kromer, B., Manning, S.W., Niu, M., Reimer, R.W., Richards, D.A., Scott, E.M., Southon, J.R., Staff, R.A., Turney, C.S.M., and van der Plicht, J., 2013. IntCal13 and Marine13 Radiocarbon Age Calibration Curves 0–50,000 Years cal BP; Radiocarbon, v. 55, p. 1869–1887. https://doi.org/10.2458/azu_js_rc.55.16947

Rutter, N.W., Minning, G.V., and Netterville, J.A., 1980. Surficial geology and geomorphology, Mills Lake, District of Mackenzie; Geological Survey of Canada, Preliminary Map 15–1978, scale 1:125 000. https://doi.org/10.4095/109708

Ruz, M.-H. and Allard, M., 1994. Foredune development along a subarctic emerging coastline, eastern Hudson Bay, Canada; Marine Geology, v. 117, p. 57–74. https://doi.org/10.1016/0025-3227(94)90006-X

Schandl, H., Fischer-Kowalski, M., West, J., Giljum, S., Dittrich, M., Eisenmenger, N., Geschke, A., Lieber, M., Wieland, H.P., Schaffartzik, A., Krausmann, F., Gierlinger, S., Hosking, K., Lenzen, M., Tanikawa, H., Miatto, A., and Fishman, T., 2016. Global Material Flows and Resource Productivity. An Assessment Study of the UNEP International Resource Panel; United Nations Environment Programme, Paris, 200 p.

Smith, D.G., 1994. Glacial lake McConnell: Paleogeography, age, duration, and associated river deltas, mackenzie river basin, western Canada; Quaternary Science Reviews, v. 13, p. 829–843. https://doi.org/10.1016/0277-3791(94)90004-3

Snyder, J., 2017. Grains of sand: How fracking has caused a surge in demand for one of the world's oldest commodities; Financial Post. <https://business.financialpost.com/commodities/energy/grains-of-sand-how-fracking-has-caused-a-surge-in-demand-for-one-of-the-worlds-oldest-commodities> [accessed September 20, 2018]

Stevens, C.W., Kerr, D.E., Wolfe, S.A., and Eagles, S., 2017. Predictive surficial geology, Yellowknife and Hearne Lake, Northwest Territories, NTS 85-J and NTS 85-I; Geological Survey of Canada, Canadian Geoscience Map 200, 2nd preliminary edition, scale 1:125 000. https://doi.org/10.4095/299516

Tarasov, L., Dyke, A.S., Neal, R.M., and Peltier, W.R., 2012. A data-calibrated distribution of deglacial chronologies for the North American ice complex from glaciological modeling; Earth and Planetary Science Letters, v. 315–316, p. 30–40. https://doi.org/10.1016/j.epsl.2011.09.010

Vanderburgh, S. and Smith, D.G., 1988. Slave River delta: geomorphology, sedimentology, and Holocene reconstruction; Canadian Journal of Earth Sciences, v. 25, p. 1990–2004. https://doi.org/10.1139/e88-186

Wolfe, S.A., 1998. Living with frozen ground: a field guide to permafrost in Yellowknife, Northwest Territories; Geological Survey of Canada, Miscellaneous Report 64, 71 p. https://doi.org/10.4095/209777

Wolfe, S.A. and Morse, P.D., 2017. Lithalsa Formation and Holocene Lake-Level Recession, Great Slave Lowland, Northwest Territories; Permafrost and Periglacial Processes, v. 28, p. 573–579. https://doi.org/10.1002/ppp.1901

Wolfe, S., Bond, J., and Lamothe, M., 2011. Dune stabilization in central and southern Yukon in relation to early Holocene environmental change, northwestern North America; Quaternary Science Reviews, v. 30, p. 324–334. https://doi.org/10.1016/j.quascirev.2010.11.010

Wolfe, S.A., Stevens, C.W., Gaanderse, A.J., and Oldenborger, G.A., 2014. Lithalsa distribution, morphology and landscape associations in the Great Slave Lowland, Northwest Territories, Canada; Geomorphology, v. 204, p. 302–313. https://doi.org/10.1016/j.geomorph.2013.08.014

Wolfe, S.A., Morse, P.D., Kokelj, S.V., and Gaanderse, A.J., 2017. Great Slave Lowland: The Legacy of Glacial Lake McConnell; *in* Landscapes and Landforms of Western Canada, (ed.) O. Slaymaker; Springer International Publishing, Cham, p. 87–96. https://doi.org/10.1007/978-3-319-44595-3_5

Wolfe, S.A., Morse, P.D., Neudorf, C.M., Kokelj, S.V., Lian, O.B., and O'Neill, H.B., 2018. Contemporary sand wedge development in seasonally frozen ground and paleoenvironmental implications; Geomorphology, v. 308, p. 215–229. https://doi.org/10.1016/j.geomorph.2018.02.015

Geological Survey of Canada Project 340545NU62